A Phoswich Detector System to Measure the $^{3}H(t,\gamma)^{6}He$ Cross Section using ICF

M. Yuly, S. Padalino, M. Coats and K. Cook

Overview of proposed experiment

One possible technique to measure low energy tritium reaction cross sections, such as $^{3}H(t,\gamma)^{6}He$, may be to use inertial confinement thermonuclear reactions followed by an in-situ radioactive decay counting experiment that happens well after the laser shot. Figure 1 shows a simplified diagram of the experiment and the associated timing. The OMEGA laser compresses and heats an ICF target causing thermonuclear tritium and deuterium reactions to occur. Mostly these will be neutron and proton producing reactions like $^{2}H(d,n)^{3}He$, $^{2}H(d,p)^{3}H$, $^{3}H(d,n)^{4}He$ and $^{3}H(t,2n)^{4}He$, but a small fraction of the time $^{3}H(t,\gamma)^{6}He$ radiative capture will occur. The ^{6}He nuclei formed in this reaction will fly out and may implant in a thin graphite shield in front of a plastic scintillator phoswich detector. The ^{6}He beta decays with a half-life of 807 ms -- which is very long compared to normal ICF time scales. This means individual ^{6}He beta decay pulses in the detector could be counted and analyzed in the relatively quiet enviroment long after the shot.

The timeline in Figure 1 shows this process. Within nanoseconds of the laser the EMP and x-rays strike the detector, followed the flash due to neutrons. During this time the PMT would be powered down and electrically isolated. A very long time later, micro- or even milliseconds later when the background is relatively low, the PMT would be connected to the counting electronics and turned on, and counting of individual pulses from the beta decay of the ^{6}He would begin. The beta energies are relatively large, so these electrons could be easily detected and identified. The signature would be to identify, event-by-event, electrons due to ^{6}He beta decay having the correct energy loss in the thin dE and thick E scintillator, with the count rate for these events exhibiting the correct decay half-life for ^{6}He.

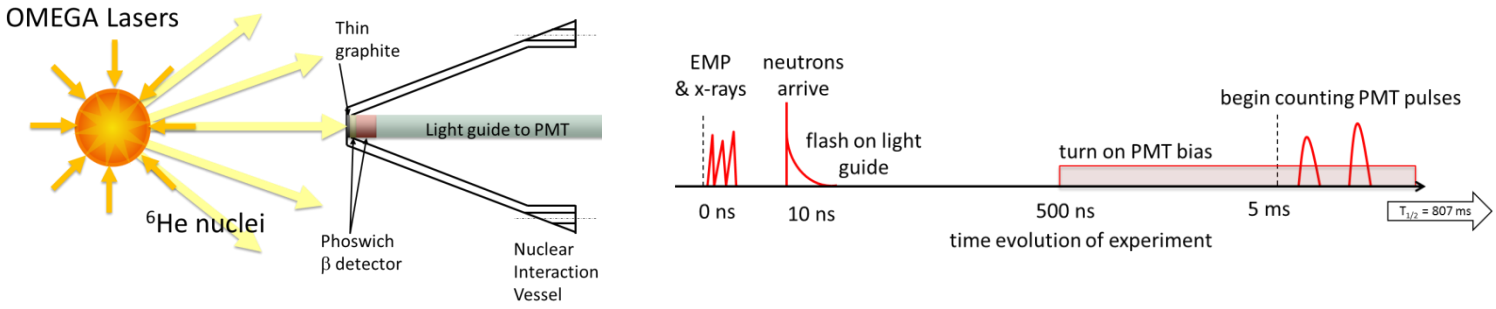

Figure 1. Simplified diagram of the proposed experiment and timing.
(Left) The ^{6}He nuclei produced by $^{3}H(t,\gamma)^{6}He$ in the ICF implosion fly outward and implant in the thin graphite shield, where they subsequently beta decay. The beta particles are counted by the phoswich detector in order to measure the decay curve and reconstruct the initial ^{6}He activity.
(Right) X-rays, neutrons and the EMP all arrive within nanoseconds of the shot, whereas the PMT will be turned on and beta decay counting will begin microseconds (or even milliseconds) after the shot.

This technique has advantages over traditional accelerator based methods and avoids the difficulties usually associated with ICF experiments. In a typical ICF experiment, the nuclear reactions occur during a few nanoseconds, which means that the signals from the detectors are not pulses associated with individual events, but at best represent an integrated signal from many reaction events. Since in this experiment the beta decay pulses are counted individually, pulse height and timing information can be extracted on an event-by-event basis and used for particle identification. Moreover, the background rate should be much lower, since these decay events occur when most of the other radiation from the implosion has died down. Conversely, since it is a thermonuclear ICF reaction, the number of interacting nuclei is very

large and the energy and the energy is low – difficult conditions to achieve with an accelerator. Furthermore, LLE routinely handles tritium, which is confined to the target chamber, thereby avoiding most of the contamination problems associated with producing tritium beams using an accelerator. .

An estimate of the count rate for this experiment can be made using the results of a recent OMEGA $^{3}H(t,2n)^{4}He$ measurement [1]. OMEGA shot numbers 55641-55647 used a 9.5 μm thick CD shell filled with 12.1 atm of DT mix containing 38.7% tritium. For these shots the average temperature was 8.0 keV and the Gamow peak energy, or the average CM reactant energy, was almost 29 keV. The total DT neutron yield and the ratio of TT to DT neutrons were both determined [2], allowing the total number of TT neutrons to be calculated. Using the highest possible realistic value for the $^{3}H(t,\gamma)^{6}He/^{3}H(t,2n)^{4}He$ branching ratio of 10^{-5} then allows the number of ^{6}He nuclei to be estimated. Assuming a target solid angle of about 30 mSr (approximately the size of the Neutron Temporal Diagnostic [3]) yields almost 20,000 ^{6}He nuclei embedded in the detector in each shot.

From this it seems like branching ratios down to about 10^{-7} might conceivably be measured using this technique. This might be improved by using an asymmetric laser shot, which would tend to push the ^{6}He ions preferentially toward the detector, artificially increasing the effective solid angle of the detector. It may also be possible to use this technique with higher energy tritons, where the cross section might be expected to by larger, by using Target Normal Sheath Acceleration (TNSA). For example, $^{2}H(d,\gamma)^{4}He$ branching ratio goes up to about 10^{-4} at 10 MeV [20]. Since the $^{3}H(t,\gamma)^{6}He$ cross section has never been measured, measurements at higher energy would still be of interest.

This technique, once developed, could also be applied to study other little-investigated low-energy nuclear reactions. For example, certain low energy tritium stripping reactions would be particularly well suited, such as $^{6}\mathrm{Li}(\mathrm{t},\ \mathrm{p})\ ^{8}\mathrm{Li}$, $^{10}\mathrm{B}(\mathrm{t},\ \mathrm{p})^{12}\mathrm{B}$, and $^{13}\mathrm{C}(\mathrm{t},\ \mathrm{p})^{15}\mathrm{C}$, all of which have final products that beta decay with half-lives of milliseconds or seconds. These would require that the target be doped with the relevant target isotope.

Motivation

The primary motivation for this experiment is that the radiative capture cross section $^{3}H(t,\gamma)^{6}He$ has never been measured -- not at any energy, not even to set an upper limit on the cross section. As far as can be determined there have not been any published calculations of the cross section for this reaction. This is true even though the reaction occurs in all DT plasma thermonuclear fusion research, and may be important for an understanding nucleosynthesis in big bang models of the early universe.

If measured, the $^{3}H(t,\gamma)^{6}He$ reaction could be used as a diagnostic [4] for high temperature DT plasmas, or, more likely since the cross section is expected to be small, could be accounted for as source of unwanted background to other diagnostic measurements made using other reactions. The use of radiative capture reactions like $^{2}H(t,\gamma)^{5}He$ and $^{2}H(d,\gamma)^{4}He$ as thermonuclear fusion diagnostics has progressed since they were first suggested [5,6], and by the present time many have been observed experimentally in plasmas at thermonuclear temperatures [7,8,9,10]

A measurement of the $^{3}H(t,\gamma)^{6}He$ cross section at low energy may also be important for understanding primordial nucleosynthesis. Current models overpredict the abundance of ^{7}Li in the early universe while simultaneously predicting to little ^{6}Li [11, 12]. One difficulty with the prediction of ^{6}Li, however, is that ^{6}He decays into ^{6}Li. Since the $^{3}H(t,\gamma)^{6}He$ cross section has not been measured its contribution is not included in these nucleosynthesis models, therefore this reaction could have a significant but unknown impact on the rate of ^{6}Li production in the early universe [13].

There are several possible reasons for this lack of experimental data on $^{3}H(t,\gamma)^{6}He$. An accelerator-based measurement of this reaction would require a tritium beam, the use of which has been discontinued at most laboratories because of

problems with tritium contamination. Even during the heydays of the 1950s and 1960s there were not many laboratories where this work could be performed. One of the last remaining examples from this period was the Los Alamos three-stage Van de Graaff Ion Beam Facility [14] which ended tritium beam production in 1994, was deactivated in 1999 [15] and decommissioned, decontaminated, and demolished starting in 2005 [16]. At the present time there are essentially no laboratories that generate intense tritium beams. To avoid radiological hazards, recent tritium-beam experiments have been forced to use very low intensity secondary beams produced via ^{9}Be(α, t) (10^6/s) [17] at NSCL, in-flight heavy-ion fragmentation of ^{16}O (5×10^6) [18] at NSCL, or very low intensity accelerated triton beams (10^8/s) using the AGOR cyclotron [19].

Another reason for the lack of experimental data is that the cross section at low energy is expected to be very small. Since the initial tritons in ^{3}H(t,γ)^{6}He are identical, the total spin 1 initial state is not allowed by the exclusion principle. This means, since the ground state of ^{6}He is 0+, that direct s-wave ($\ell = 0$) scattering to the ^{6}He ground state, which might be expected to be the largest reaction channel, is forbidden by angular momentum conservation (0+ → 0+). Other reaction pathways may be possible, but with much lower probability. These include scattering of higher orbital angular momentum incident waves giving an increased angular momentum barrier, transitions to other excited states of ^{6}He, and resonance transitions and resonant capture through other channels than ^{3}H+^{3}H. Another possibility that could increase the cross section might be the incorrect assignment of the angular momentum of a ^{6}He state or an admixture, as was the case for ^{2}H(d, γ)^{4}He [20,21]. For example, studies of ^{3}He(^{3}He ,γ)^{6}Be mirror reaction show that reaction proceeds primarily through the first excited state of ^{6}Be [22,23]. Unfortunately, the first excited state of ^{6}He primarily decays through α + 2n, which does not result in ^{6}He in the final state. One approach to calculating the cross section for ^{3}H(t,γ)^{6}He is to use R-matrix theory. Work on this has started using the code AZURE2, which allows multichannel, multilevel R-matrix calculations of cross sections for resonant nuclear reactions, including radiative capture [24].

Initial experiments to create and detect ^{6}He

Last summer a silicon detector telescope (which was described in detail in the 2016 report) was built for the purpose of testing whether we could create and detect ^{6}He, but only preliminary results were obtained. At the start of this summer, an improved measurement was made using the same silicon detector telescope, but with updated firmware for the FemtoDAQ data acquisition system. Last summer the FemtoDAQ had to be read out after each event, so the dead time was very large. The new firmware allowed the FemtoDAQ to store the time stamp and pulse height information for each event locally on the FPGA, which was then read out at the end. This new system has very little dead time, although the actual value has still not been determined.

The detector telescope consisted of a very thin transmission-mount silicon surface barrier dE detector in front of a much thicker surface barrier E detector. Even so, most beta particles from the decay of ^{6}He had enough energy to punch through the E detector. This occurred starting at a beta energy of about 1.6 MeV. Moreover, the dE detector was so thin that the beta particle pulses were only a little larger than the phototube noise.

A diagram of the experiment and photographs of the detector telescope and target chamber are shown in Figure 2. An approximately 110 nA beam of 2.0 MeV deuterons entered the chamber and struck a 0.36 mm thick deuterated polyethylene sheet. The beam was collimated to 3.175 mm in diameter just upstream of the target chamber. The burn marks on the polyethylene in Figure 2 are evidence that the beam was striking the target although perhaps not quite centered. Behind the deuterated polyethylene was a 19.5 mm by 26 mm by 6.5 mm thick rectangular plate of ^{9}Be. Neutrons produced by ^{2}H(d,n)^{3}H reacted with the ^{9}Be to produce ^{6}He via ^{9}Be(n,α)^{6}He. The ^{6}He nuclei, embedded in the ^{9}Be, beta decayed with a half-life of 807 ms. The resulting beta particles penetrated out of the ^{9}Be and were detected by the dE-E telescope.

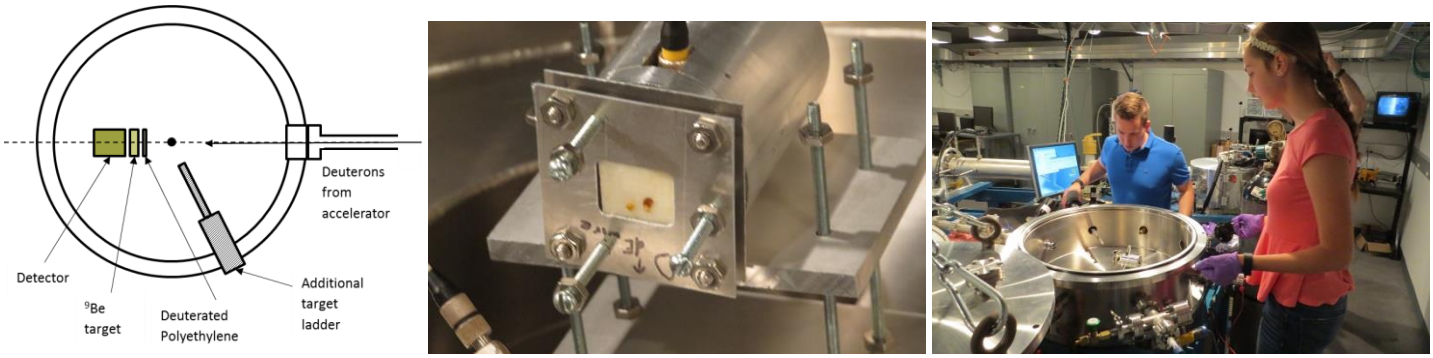

Figure 2. Preliminary experiment to measure ^{6}He half life.
(Left) Diagram of the experiment. Deuterons entered the target chamber and struck a thin sheet of deuterated polyethylene. Neutrons released by ^{2}H(d,n)^{3}He reactions in the polyethylene struck a ^{9}Be plate, which resulted in ^{6}He forming via ^{9}Be(n,α)^{6}He. The silicon detector telescope counted the resulting ^{6}He beta decay events.
(Center) The silicon detector telescope and target holders. The dark marks on the polyethylene were caused by deuteron beam heating.
(Right) The target chamber. Houghton student Katelyn Cook and SUNY Geneseo student Ryan Ward installing the detector in the target chamber.

The data collecting procedure took about 15 seconds, but was repeated many times to collect more statistics. First, one of the upstream faraday cups was removed to allow the deuteron beam to strike the deuterated polyethylene for 5 seconds. The cup was then reinserted, blocking the beam, and beta decay events were counted as a function of time for 10 seconds. Since the procedure was carried out by hand and since it was not known precisely when or how quickly the cup blocked the beam, from run to run there was found to be about 0.5 seconds of jitter in when the beam was stopped. In order to line up the decay curves, the data from each run were histogrammed into 10 ms bins and offsets determined by hand to align the sharp beam cut-off edges to time t=0. The falling edge of the beam was found to be at most about 20-30 ms long. Based on the speed of the actuator and the size of the beam spot the time needed to completely block the beam could be estimated to be a few milliseconds.

Figure 3 shows the pulse height spectra obtained (using the ^{9}Be target and summing over 25 repetitions) for events after time t=0. The upper left histogram is the dE spectrum, which shows relatively good separation of noise (lower peak) from beta particles (upper peak). The upper right histogram shows E detector pulse heights. The lower plot shows dE and E as a 2D histogram. The clear separation between good electron events and noise can be seen in the 2D histogram, and improves with increasing energy deposited in the E detector. Electrons entering at an oblique angle could deposit more energy in the E detector than the punch-through energy at 1.6 MeV. Events with dE greater than channel 360 and E greater than channel 500 were considered good electron events and counted as a function of time after t=0.

The top plot in Figure 4 shows the number of counts in 100 ms time bins for good electron events in the dE-E window described above. The large number of counts for times t<0 results from the beam hitting the target. In order to explore the consequences of the uncertainty in when the Faraday cup was fully inserted, an exponential decay curve was fit to the decay curve for data between a starting bin (which was allowed to vary) and 10 seconds. The middle plot shows χ^2/degree of freedom for the fit as a function of the starting bin. Immediately after t=0 the value of χ^2/degree of freedom is approximately 1.0, indicating a good fit, but slowly increases as the starting channel for the fit is increased. The best fit was obtained with the fit starting time t = 100 ms, shortly after t=0, which makes sense given the uncertainty in the time when the beam was stopped.

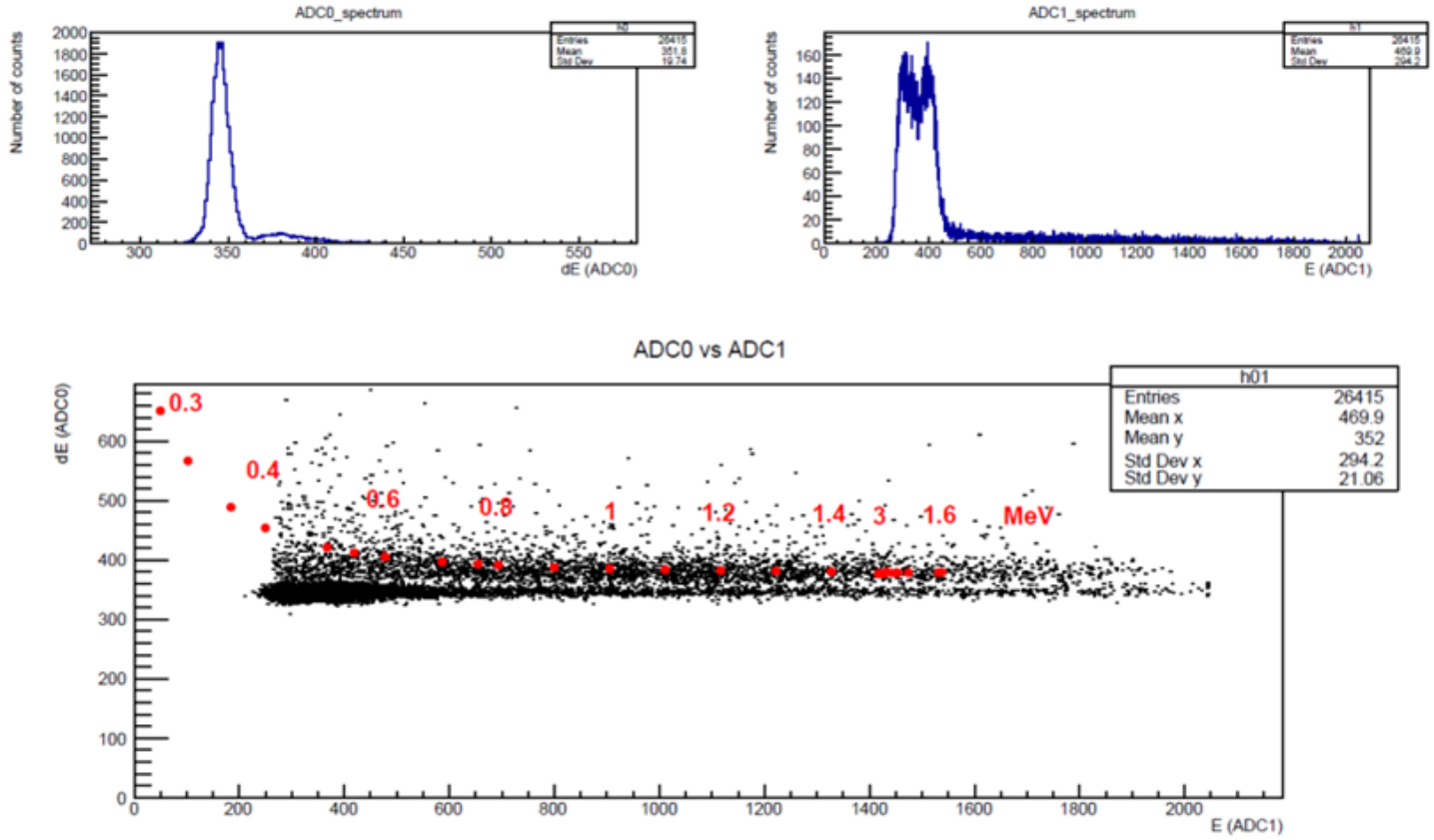

Figure 3. The dE and E singles energy spectrum histograms (top left and right respectively) and the dE-E 2D histogram (bottom). The red points and numbers on this histogram show an approximate energy calibration made using a ^{68}Ge beta source and a ^{207}Bi internal conversion source and using projected range for electrons in silicon, calculated using ESTAR [25].

The bottom plot in Figure 4 shows the fit value of the half-life obtained as a function of starting channel for the fit. The red line shown is 806.7 ± 1.5 ms, which is the previously measured value [26]. Half-life values for fit starting times t<0 are nonsense because new ^{6}He is being created by the beam. For times t>=0 the fit half-life is approximately constant with increasingly large error bars as the quality of the fit is reduced as fewer data appoints are included in the fit. The best fit ^{6}He half-life value is 0.818+/-0.018 s, which is consistent with the previously measured value. The best-fit decay curve is plotted (red) in the top histogram of Figure 4.

As an additional check, the ^{9}Be target was replaced with a 34.5 mm by 19.5 mm by 6 mm thick graphite plate. For this target, the count rate fell to zero within 0.05 seconds of when the Faraday cup was reinserted; no 0.807 s half-life decay curve was visible.

Design and construction of a phoswich detector

Having demonstrated the ability to create and detect ^{6}He using the silicon detector telescope, the next step was to design and test a detector that could survive inside the target chamber during an ICF shot. A phoswich detector was selected because of the desire to have a thin dE scintillator followed by a thick E scintillator to allow for particle identification. The phoswich design allows much more light to be collected than would be possible by attaching a separate light guide to the thin edge of the dE detector, and also has the advantage of only requiring a single light guide and phototube.

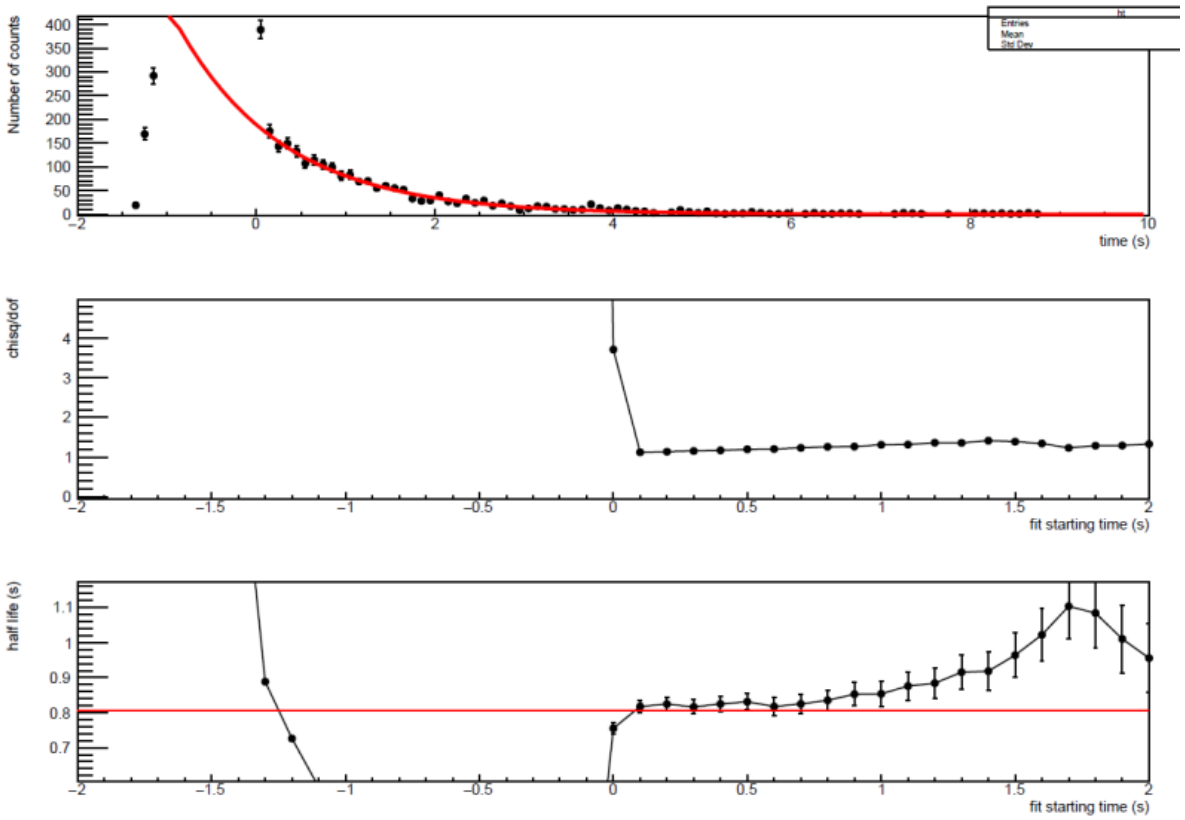

Figure 4. Decay curve for 6He. (Top) Number of beta decay events histogrammed into 10 ms time bins for 10 seconds. (Center) The value χ^2/degree of freedom for fits starting on the indicated time bin. (Bottom) The resulting fitted half-life for fits starting on the indicated time bin. The red line shows the previously measure value of 0.807 seconds for the half-life of ^{6}He.

Conceptually, the detector operates as shown in Figure 5. The ^{6}He nuclei from the ICF implosion fly out and implant in the thin graphite shield. They then beta decay releasing electrons with a typical beta spectrum having endpoint energy 3508 keV and average energy 1567 keV [26]. After losing a small amount of energy exiting the graphite, the beta particles deposit about 0.2 MeV (for velocities perpendicular to the dE surface) in a 1.0 mm thick, 1.0 cm diameter BC-408 plastic scintillator dE detector having a decay time of 2.1 ns. They then enter the 17.0 mm thick, 1.0 cm diameter BC-444 plastic scintillator where they stop unless they exit through one of the side edges. The decay time for BC-444 is 285 ns. Light from both scintillators enters the photomultiplier tube simultaneously.

The plastic scintillators are attached to each other and the photomultiplier using optical grease, and are held in place by a 3D printed light shield made from black ABS plastic, shown in Figure 6. This keeps ambient light from entering the PMT, keeps the scintillators in place, and also holds a test source or the ^{9}Be target in from of the dE scintillator. Aluminum foil 0.017 mm thick covers the entrance of the detector, which is the face of the dE scintillator, in order to complete the light tight seal.

We tested four different 2-inch phototubes, each with the appropriate base selected from ORTEC 265 (21 pin), ORTEC 269 (20 pin), ORTEC 297 (14 pin) and two homemade designs. For each phoswich/PMT/base combination pulses were generated using an ^{241}Am alpha source to look at dE scintillator performance and a ^{207}Bi internal conversion electron source, which gives nearly monoenergetic 1 MeV electrons, to test the E scintillator tail. Many of the PMT/base combinations exhibited some ringing on the long tail. Because of the sensitivity of the E detector signal on the particular shape of the BC-444 decay tail, PMT/base combinations that exhibited ringing were immediately eliminated. Table 1

shows that it was also important to have adequate gain, which eliminated the 10-stage tube. The best performing pair was the Photonis XP2262 12 stage tube with the ORTEC 269 base, the runner-up was the Burle 8575 12 stage tube with the ORTEC 265 base.

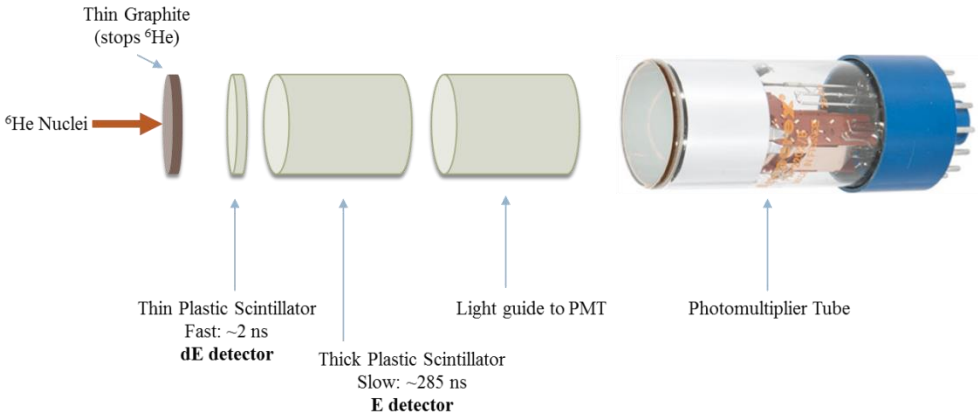

Figure 5. An exploded view diagram of the phoswich detector. The ^{6}He nuclei implant in the thin graphite shield where they decay. The resulting beta particles may deposit energy into the thin dE scintillator and the thick E scintillator. Light from both scintillators passes through the light guide and is detected by the photomultiplier tube. The detector currently does not include the light guide.

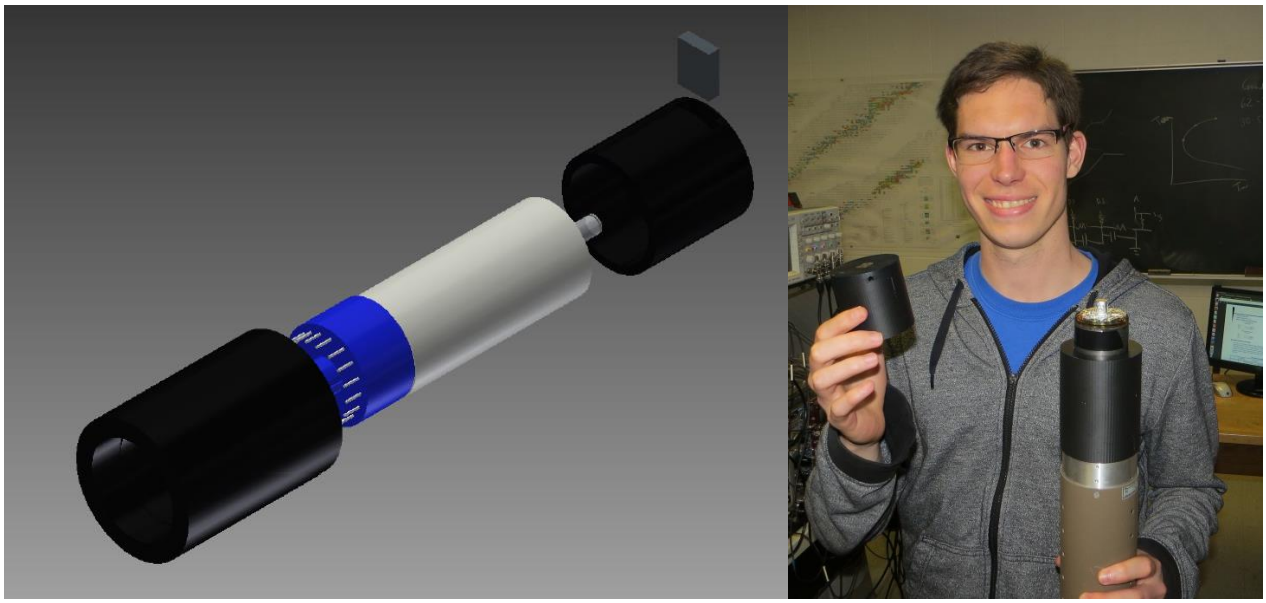

Figure 6. (Left) An exploded CAD drawing of the detector system, including the 3D printed plastic light shield and target holder. A beta source or rectangular ^{9}Be target (shown) slides into a pocket in front of the dE scintillator. (Right) Houghton undergraduate student Micah Coats holding the completed detector assembly. The plastic scintillators are covered with aluminum foil to make a light tight window over the end of the scintillator.

Figure 7 shows typical pulses obtained using the ^{207}Bi conversion source. The leftmost oscilloscope trace was made with only the 1 mm thick BC-408 dE scintillator attached to the phototube. The pulse is very short as would be expected for the 2.1 ns decay time for BC-408. The center oscilloscope trace shows a typical pulse obtained with just the 13 mm thick BC-444 E scintillator. The leftmost trace shows both scintillators operating as a phoswich. Here the fast dE and long E

tail can be distinguished and used to extract the energy deposited in each scintillator. The red line shows the approximate linear gate cut that was used for this purpose.

Table 1. Results of photomultiplier tube testing. The two phototubes listed in red were selected as the best performing tubes for this application.

PMT	Base	Ringing	Alpha Pulse (mV)	Beta Pulse (mV)	Tail Height (mV) / Scintillator Sizes		Supply Voltage (V)	Gain	Stages
XP2262	269	N	50	600	75	1mm/13mm	-1800	10^7	12
XP2202	296	Y	40	200	5	2mm/15mm	1100	10^6	10
XP2202	Homemade (NNC)	N	-	220	10	2mm/15mm	1250	10^6	10
XP2202	Harshaw	Y	50	200	5	2mm/15mm	1250	10^6	10
8575	Homemade (LANL)	Y	100	220	5	2mm/15mm	-1500	10^7	12
8575	265	N	800	1000	50	2mm/15mm	-2000	10^7	12
56AVP	269	Y	180	400	20	2mm/15mm	-2000	10^8	14

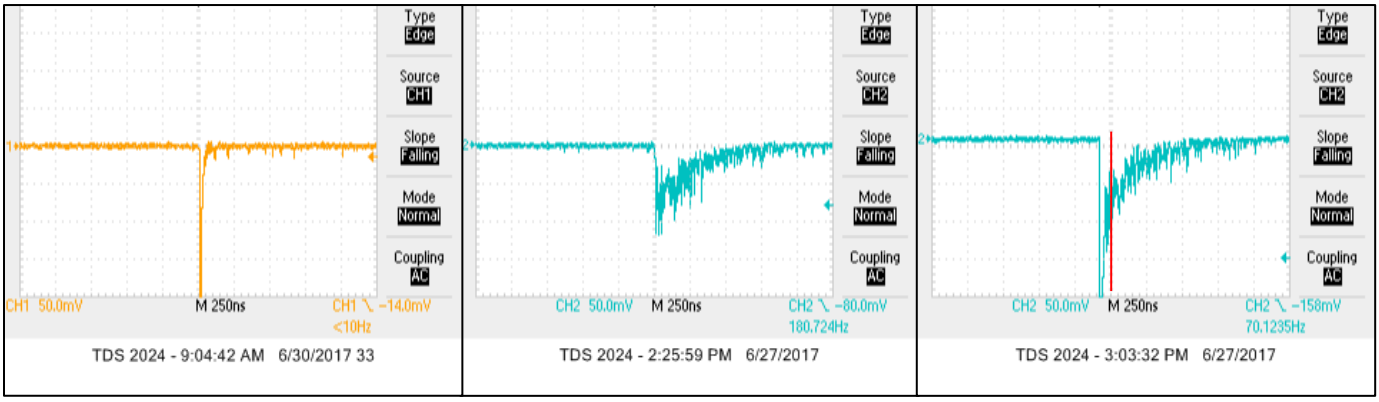

Figure 7. Oscilloscope traces for the dE detector alone (left), for the E detector alone (center), and for the dE-E phoswich combination (right). The red line shows the approximate position of the cut used to separate dE and E pulse height information.

The circuit shown in Figure 8 was used to extract the dE and E pulse height information for each event. The Lecroy 428F linear fan-out was used to split the signal from the PMT anode into three paths. One of the anode signals was used to trigger the FemtoDAQ whenever there was a pulse, and to form the logic gate used by the EG&G LG105/N linear gate and stretcher NIM module to select the E tail. The gate generator was used to delay the trigger so that it came at an appropriate time relative to the dE and E FemtoDAQ inputs. The other two anode channels were delayed by 32 ns so that the rising edge of logic gate input to the LG105/N linear gate fell at about the same position in time relative to the anode pulse as the red line in Figure 7. The logic gate was approximately 400 ns long to include the majority of the E tail. Because of the input requirements of the LG105/N linear gate module, the input signal was attenuated by 6 dB.

The linear gate output, which because of the pulse stretcher function of the LG105/N was an analog pulse with maximum amplitude proportional to the maximum signal during the logic gate window and was therefore also proportional to the energy deposited in the E detector, was sent to input B of the FemtoDAQ digitizer. The last anode signal was delayed by 128 ns so that it was input into FemtoDAQ input B at close to the same time as the E signal from the linear gate. Since this was the raw anode signal, the FemtoDAQ digitized the maximum pulse height which was the dE pulse height.

Several tests of the phoswich detector and the circuit shown in Figure 8 were carried out using a ^{207}Bi internal conversion source, which releases monoenergetic 482, 554, 976, and 1048 keV electrons, and the ^{68}Ge source, which has a beta spectrum with an endpoint of about 1.9 MeV. Figure 9 shows the dE-E 2D histograms obtained for different sources and collimation. The red dots show approximately where electrons with that energy would fall if they hit normal to the dE surface, calculated using ESTAR [25] and approximately calibrated using the ^{207}B peak at about 1 MeV (i.e. the peaks at 976 and 1048 keV merge because of straggling). The events around E=0 could be either low energy particles that stop in the dE scintillator or the edge of the dE pulse spilling into the E linear gate window for very large dE pulses.

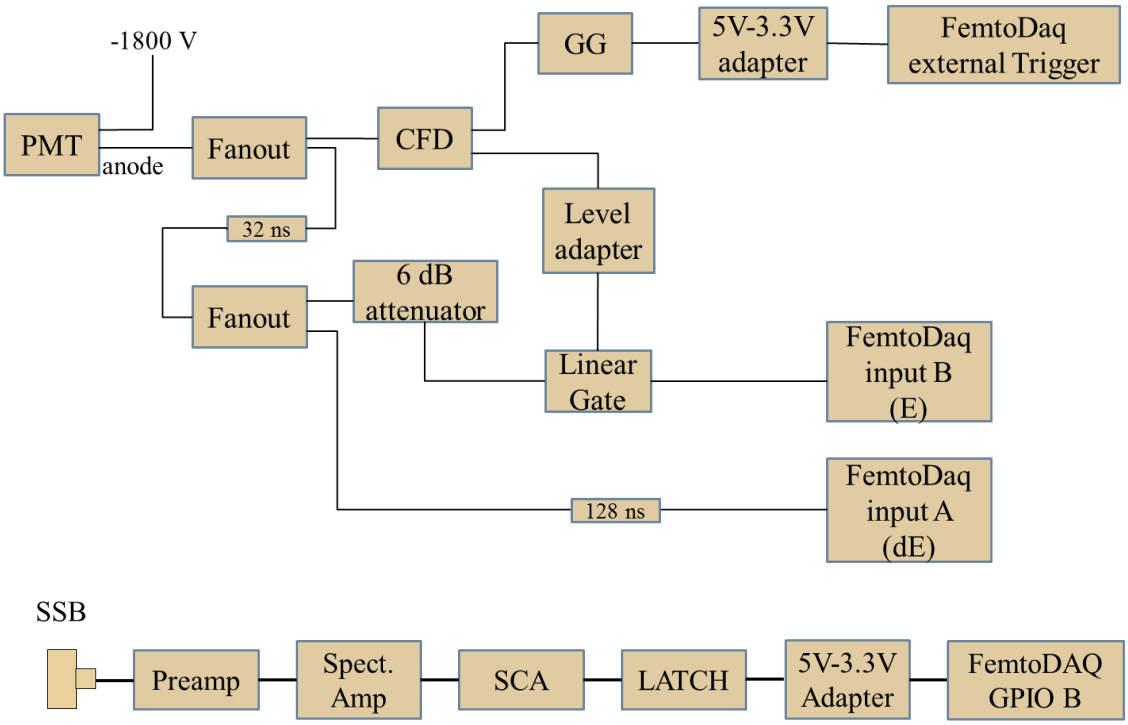

Figure 8. (Top) Block diagram of the NIM electronics used to select the dE and E components of the PMT anode pulse. The anode pulses were split into three paths. One was used to generate the trigger and gate input for the linear gate. The other two formed the dE and E inputs to the FemtoDAQ digitizer. (Bottom) The NIM circuit used to detect when the beam stopped hitting a gold elastic scattering target. This circuit told the FemtoDAQ when it was time to start counting the ^{6}He decay curve. CFD = constant fraction discriminator, GG = gate generator, SCA = single channel analyzer.

The top dE-E 2D histogram in Figure 9 shows the room background, and was made with no source or collimator in front of the dE detector. It is still possible to make out the band corresponding to electrons, but there are very few. The middle histogram shows the result obtained with the collimated ^{207}Bi source. The source was collimated by placing a 38.1 mm long 25.1 mm diameter steel cylinder with a 12.7 mm diameter hole drilled along its axis between the source and the detector. At the end of the collimator nearest the detector was a 6 mm thick brass plug with a 5.1 mm diameter hole through which the electrons had to pass to reach the detector. It is very clear that the electrons fall along the

expected band, and the peak at about 1 MeV is visible but broadened. Because the dE plastic scintillator is much thicker than the dE silicon surface barrier detector used previously, and also because of the intrinsic energy resolution of plastic scintillator relative to silicon, the overall energy resolution is much worse with the plastic scintillator. This disadvantage is somewhat ameliorated by the much larger pulses obtained as a result of the greater dE thickness.

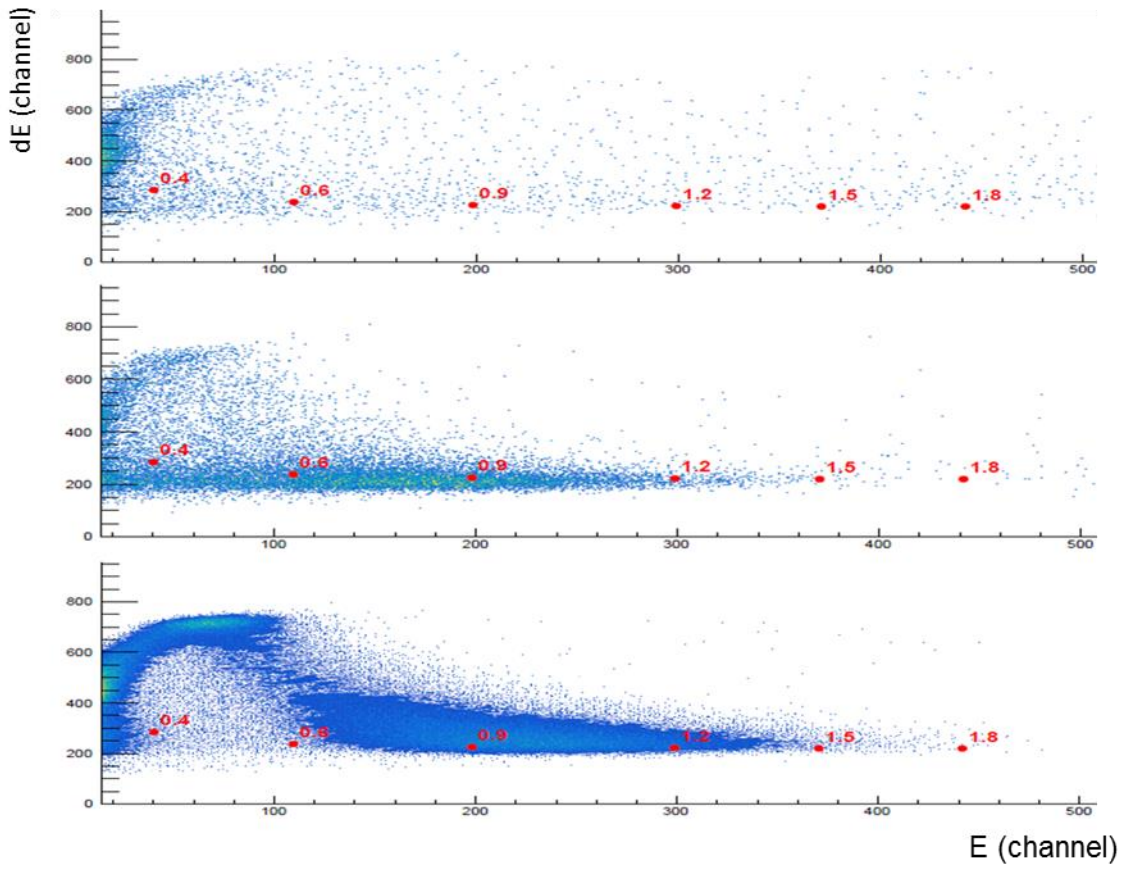

Figure 9. 2D histograms of dE versus E scintillator pulse heights for background (top), a collimated ^{207}Bi source (middle) and an uncollimated ^{207}Bi source (bottom).

The bottom histogram in Figure 9 shows the results without the collimator, when the ^{207}Bi source was placed directly on top of the dE scintillator. In this case, it is possible for the electrons to enter the dE detector at an angle rather than only along the normal. These electrons will depot more energy in the dE scintillator and correspondingly less in the E scintillator, moving these events upward and toward the left on the 2D histogram. The results were similar but more difficult to interpret using the ^{68}Ge source, because of the smoothly varying beta spectrum does not have any peaks.

Phoswich test experiment

In the near future we intend to take the phoswich detector to SUNY Geneseo to carry out a test experiment similar to the one described earlier using the silicon detector telescope. Figure 10 shows the planned layout of the target chamber for the experiment. The collimated deuteron beam will first encounter a 0.1 μm thick gold foil at 45° to the beam. Deuterons elastically scattered at 90° from the foil will be detected by a silicon surface barrier detector (SSB). Pulses from this detector will be used to signal to the computer when the Faraday cup is in and out for the purpose of automating the data collection procedure. The majority of the deuterons will pass through the gold foil and strike the deuterated polyethylene located at the far back side of the scattering chamber, producing neutrons via ^{2}H(d,n)^{3}He. These neutrons will penetrate the 2.75 inch conflat glass viewport to reach the ^{9}Be plate located just outside, in the air.

The neutrons will induce the $^{9}Be(n,\alpha)^{6}He$ reaction resulting in embedded ^{6}He nuclei which will then beta decay. The resulting beta particles will be detected by the phoswich detector.

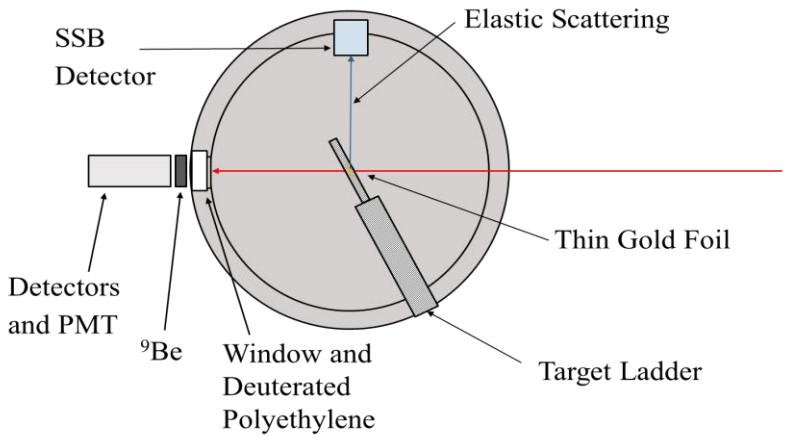

Figure 10. Diagram of the experiment to test the phoswich detector. Deuterons entering the chamber will first pass through a thin gold foil. Some of them will scatter elastically from the gold and will be detected by a SSB detector used to monitor the beam. The rest will strike the thin deuterated polyethylene foil at the far end of the target chamber. Neutrons released from the polyethylene will penetrate a window and strike the ^{9}Be target, creating 6He. The ^{6}He decays will be detected by the phoswich detector.

The bottom diagram in Figure 8 shows a block diagram of the NIM circuit that will be used to automate data collection. The presence of pulses from the SSB detector will indicate that the Faraday cup is out and the beam is hitting the polyethylene. These pulses will first be shaped and amplified using a standard NIM preamplifier and spectroscopy amplifier. The Single Channel Analyzer (SCA) will produce logic pulses whenever the SSB pulse is larger than a certain threshold. The "LATCH" module is a homemade NIM module containing the circuit shown in Figure 11, a retriggerable monostable multivibrator circuit. For each input logic pulse to the LATCH circuit, an output logic pulse of an adjustable length will be produced. Another input pulse coming before the end of this output pulse will simply restart the output pulse, again with the same width. The LATCH output will therefore be continuously high unless a period of time longer than the set output logic pulse width elapses without an input pulse.

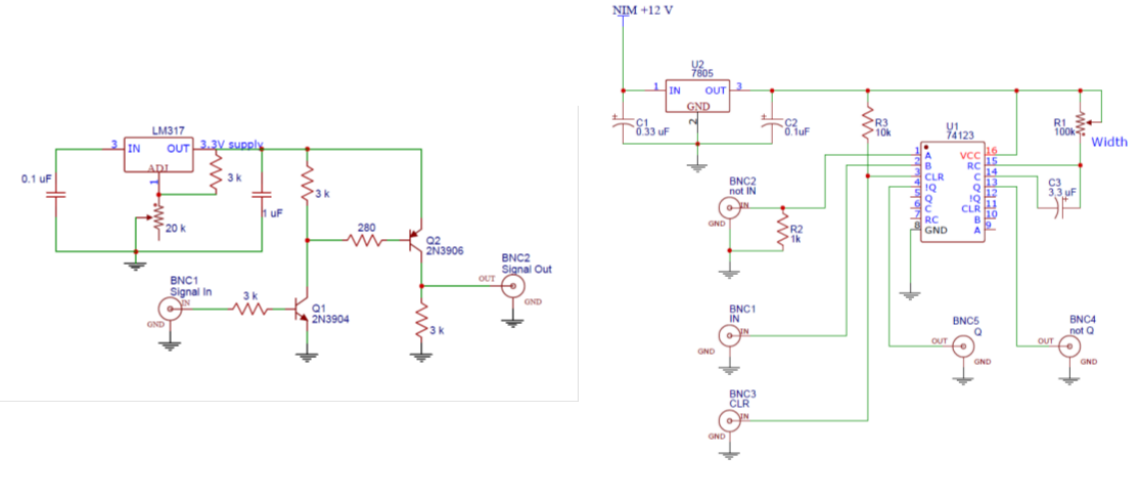

Figure 11. Schematic diagrams of the "5-3.3 V converter" (left) and "LATCH" (right) circuits used in Figure 8. These were constructed in NIM-standard enclosures for use in our NIM bins.

The FemtoDAQ will be programmed to continuously watch the GPIO B logic input. As long as it remains high, it will know that the Faraday cup is out and the beam is hitting the target. It will wait for 5 seconds, and then alert the accelerator operator that the Faraday cup should be inserted, stopping the deuteron beam. As soon as the FemtoDAQ sees the GPIO B input go low, it will collect data for 10 seconds. At the end of this period, it will read out and store the collected event list from the FPGA, then indicate to the accelerator operator that it is ready to have the Faraday cup removed again, allowing the beam to strike the target. This process will be repeated as many times as possible to collect statistics.

Summary and Future Plans

It has been demonstrated that we can produce ^{6}He using the ^{9}Be(n,α)^{6}He reaction, identify the ^{6}He beta electrons, and measure the ^{6}He half-life with a silicon detector telescope. A phoswich dE-E detector system has been developed, and will be tested in a few weeks. Assuming that this test is successful, the next step would be to adapt the phoswich detector to be tested in a series of ride-along shots using the OMEGA laser. Before requesting dedicated shots to attempt a measurement of ^{3}H(t,γ)^{6}He or one of the tritium stripping reactions mentioned earlier, there are several questions that still must be addressed:

1. *What is the best size, positon and configuration for the phoswich detector?*

We are working with LLE engineer Chuck Sorce to address of these questions. The original proposal was for the phoswich detector to have the same diameter and distance from the target as the plastic scintillator used for the Neutron Temporal Diagnostic (NTD). Since then we have learned that the detector will most likely need to be about 20 cm away, or 10 times farther than originally thought, in order to avoid ablation of the graphite shield. Since it is crucial for the experiment that the ^{6}He nuclei implant in the graphite, it currently does not seem prudent to have the shield too close to the target center. To keep the same solid angle as the NTD would then require a detector with about 100 cm^{2} of active area.

2. *How far away must we place the PMT and the electronics?*

This question is associated with the previous question. It would be very beneficial to have the PMT as close as possible to the plastic scintillator. If it will work within a short enough distance that we can use a solid acrylic light guide between the scintillator and the PMT, much more of the scintillation light will be collected, which would be very helpful in terms of dE-E particle identification and was the primary advantage of using a phoswich detector in the first place. If we are forced to locate the PMT farther away, then we will need to use either a very think bundle of fiber optics as a light guide or lose a significant portion of the light.

3. *If we electrically isolate the PMT, can we place it immediately outside the chamber?*

This question is in turn associated with the previous question. Since we are not interested in obtaining a useable signal within nanoseconds of the shot, but rather micro- or even milliseconds, would it be sufficient to place the PMT just outside the target chamber if it was completely electrically isolated? To test the feasibility of this idea, an experiment was performed in which the high voltage was electrically disconnected from a PMT by a high voltage switch. Simultaneously, we had the PMT anode connected to a preamplifier and spectroscopy amplifier with the longest time constant possible, producing almost 50 μs long bipolar pulses so we could see them on a millisecond oscilloscope time scale. The oscilloscope screen shot in Figure 12 (left) shows that the high voltage takes only about 5 milliseconds to stabilize, and anode pulses are visible shortly thereafter. These times were very consistent every time the high voltage was connected. The screen shot on the right is zoomed in on one of the detector pulses. When the radioactive source was taken away, these pulses immediately following the HV turn-on disappeared, lending credence to the idea the PMT

becomes active within 10 ms of connecting the high voltage. This indicates it may be possible for the PMT to be located close to the chamber, and the power switched on by using a high voltage relay in order to completely electrically isolate the PMT from the electronics, and that it could be done in less than 10 ms.

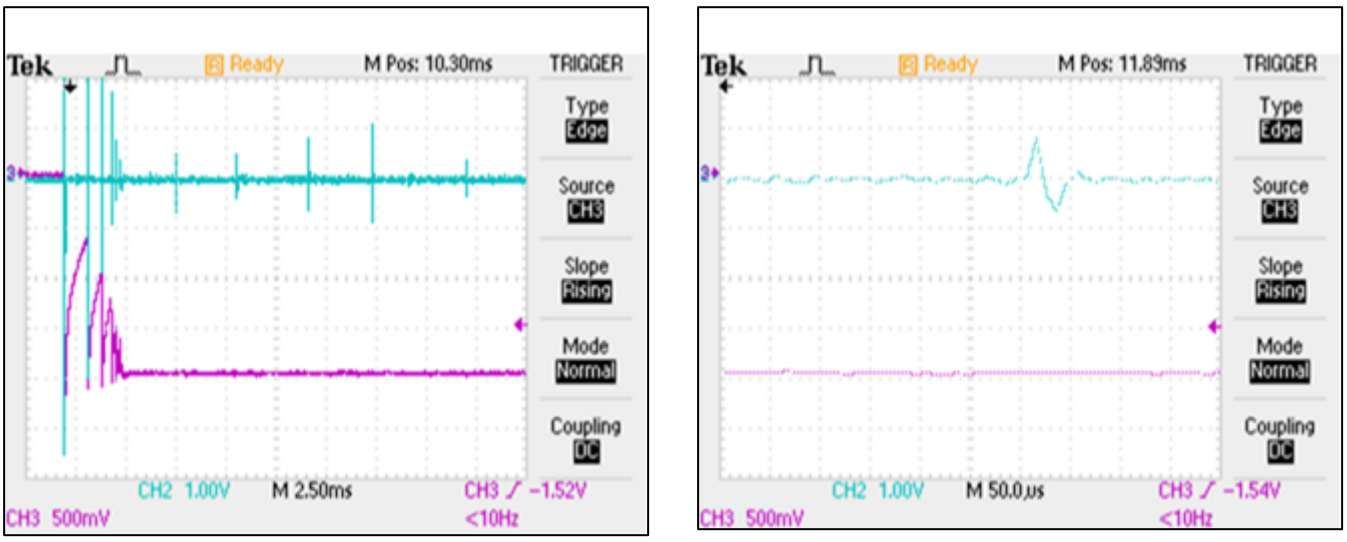

Figure 12. Oscilloscope traces for the PMT high voltage (pink) measured using a x1000 high voltage probe and the anode pulse output from the spectroscopy amplifier (blue) for a 25 ms full scale (left) and 500 μs full scale (right).

4. How much energy will the ^{6}He have when it hits the graphite and how long will the ^{6}He stick to the graphite?

Simple conservation of energy yields about 13.5 keV for the outgoing ^{6}He nucleus from the ^{3}H(t,γ)^{6}He reaction. What is not known, however, is how much energy the ^{6}He will lose in the plasma as it leaves the target. A future project would be to simulate this with the goal of predicting the kinetic energy distribution of the ^{6}He nuclei as they reach the detector, and the degree of isotropy in the spatial distribution.

Other researchers have studied the desorption of ^{4}He implanted into graphite [27,28,29] and found that "in the case of POCO graphite (i.e. isotropic graphite sheet) studied here, only a few percent of retained helium will be released by the annealing up to 200°C, except for that of lower doses [28]." Figure 13 shows that the peak desorption for a irradiation doses of 5×10^{17} ions/cm^2 is about 10^{-5} STP cm^3/min, which is roughly 5×10^{12} atoms/s. While the paper does not say the size of the sample, if it was 1 cm^2 this would mean only 0.001% of the atoms were desorbed each second even at the peak temperature.

While this in encouraging, of course this experiment *would* have much lower dose rates, ^{6}He instead of ^{4}He, and much shorter timeframes (i.e. seconds rather than minutes). It may be possible to study the desorption of ^{4}He ions from graphite at much lower dosage rates and energies, i.e. similar to our experiment, with the same technique as Ref. [28] by using the SUNY Geneseo duoplasmatron and a residual gas analyzer. For ^{6}He desorption rates, it may be possible to measure this using the ^{9}Be(n,α)^{6}He reaction in very thin graphite foils doped with ^{9}Be, where the SUNY Geneseo pelletron would be used to create the neutrons and the phoswich or silicon detector would be placed in a location where beta particles from the foil could not reach the detector, but those coming from desorbed ^{6}He nuclei that have left the graphite surface before subsequently decaying could reach the detector.

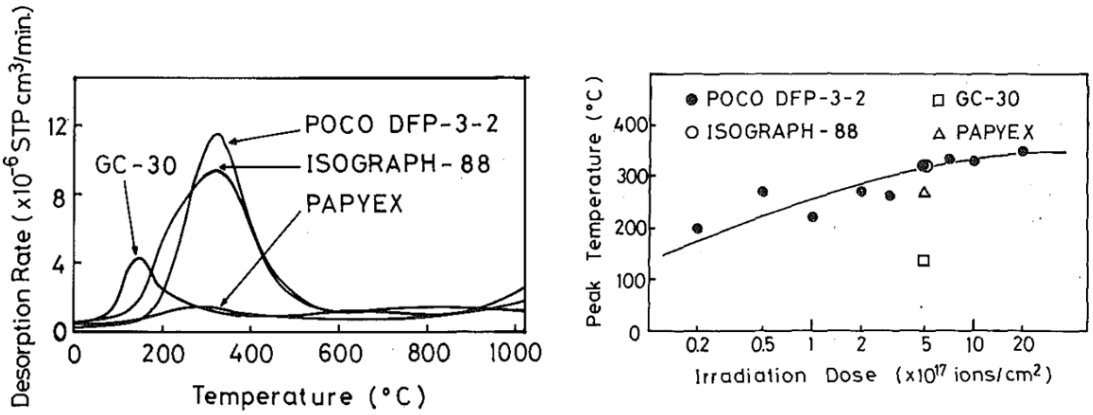

Figure 13. (Left) Thermal desorption curves of ^{4}He from various graphite samples irradiated with 20 keV He^{+} ions at a dose of 5.0×10^{17} ions/cm^2. (Right) Change in peak desorption temperature with irradiation dose for various graphite samples. Figures taken from Ref. [28].

5. *What does the background look like for the 5 seconds after the initial pulse?*

To answer this question, we would need a ride-along test shot. The detector would be placed in the OMEGA chamber, and measurements of the background rate and dE-E distribution could be made as a function of time -- spanning the range from about 10 ms after the shot until several minutes.

6. *What is the efficiency of our detector?*

The answer to this question is needed in order to convert the ^{6}He beta decay curve into an absolute cross section measurement. One idea for how to do this is to normalize using the previously measured $^{9}Be(n,\alpha)^{6}He$ cross section at 14.1 MeV. By placing a thin ^{9}Be foil over the end of the phoswich detector, primary DT neutrons would create a known number of embedded ^{6}He nuclei in very close to the same geometry as the nuclei embedded in the graphite shield from $^{3}H(t,\gamma)^{6}He$.

Presentations made since Summer 2016

Micah Coats, Katelyn Cook, Mark Yuly, Stephen Padalino, Craig Sangster and Sean Regan. "Measurement of the ^{6}He Decay Produced by the $^{9}Be(n,\alpha)^{6}He$ Reaction"

1. Omega Laser User's Workshop, Laboratory for Laser Energetics, Rochester, NY, April 26, 2017, Best Poster Award.
2. XXXVI Annual Rochester Symposium for Physics Students, University of Rochester, Rochester, NY., April 1, 2017.
3. 58th Annual Meeting of the APS Division of Plasma Physics, San Jose, CA, Oct. 31 - Nov. 4, 2016, Outstanding Undergraduate Poster Award.

This material is based upon work supported by the Department of Energy [National Nuclear Security Administration] University of Rochester "National Inertial Confinement Program" under Award Number(s) DE-NA0004144.

---

[1] D. T. Casey et al., Phys. Rev. Lett. **109**, 025003 (2012).
[2] D. T. Casey, Ph.D. Thesis, Massachusetts Institute of Technology (2012). (PSFC/RR-12-1)
[3] C. Stoekl et al., Rev. Sci. Instrum. **87**, 053501 (2016).
[4] V.G. Kiptily, F. E. Cecil, and S. S. Medley. Plasma Physics and Controlled Fusion **48**, R59 (2006).
[5] S.S. Medley and H. Hendel, Princeton Plasma Physics Laboratory Report #1950 (1980).
[6] F.E. Cecil and D.E. Newman, Nucl. Instrum. Methods. **221**, 449 (1984).
[7] Y. Kim et. al., Phys. Rev. **C85**, 061601 (2012).
[8] D.A. Boyd, D.J. Campbell, J.G. Cordey, W.G.F. Core, J.P. Christiansen, G.A. Cottrell, L.G. Eriksson, T. Hellsten, J.J. Jacquinot, O.N. Jarvis, P.R. Thomas, P. v. Belle, and J.A. Wesson, Nuclear Fusion **29,** 593 (1989).
[9] F.E. Cecil and S.S. Medley, Nucl. Instrum. Methods **271,** 628 (1989).
[10] T. Nishitani, K. Tobita, Y. Kusama, and Y. Shibata, Rev. Sci. Instrum. **72**, 887 (2001).
[11] J. Melendez and I. Ramirez, Astrophys. J. **615**, L33 (2004).
[12] M. Asplund et al., Astrophys. J. **644**, 229 (2006).
[13] M. Kanga, Y. Hub, H. Hua and S. Zhub, Journal of Cosmology and Astroparticle Physics **2012**, 011 (2012).
[14] R. Woods, J.L. McKibben, and R.L. Henkel, Nuclear Instruments and Methods **122**, 81-971 (1974).
[15] United States Government Accountability Office, Report to the Committee on Armed Services, U.S. Senate, Report GAO-15-272, 2015.
[16] Loomis et al., Los Alamos National Laboratory Report LA-UR-05-0775, 2005.
[17] B. M. Sherrill et al., Nucl. Instrum. Methods **A 432**, 299 (1999).
[18] G. W. Hitt et al., Nucl. Instrum. Methods **A 566**, 264 (2006).
[19] S. Brandenburg *et al.*, in *Cyclotrons and Their Applications 2001*, proceeding s of the 16th International Conference on Cyclotrons and Applications, edited by F. Marti (American Institute of Physics, 2001), p. 463.
[20] F.J. Wilkinson III and F.E. Cecil, Physical Review **C31**, 2036 (1985).
[21] C.A. Barnes, K.H. Chang, T.R. Donoghue and C. Rolfs, Physics Letters **B197**, 315 (1987).
[22] W. D. Harrison et al., Phys. Rev. **160**, 160 (1967).
[23] E. Ventura et al., Nucl. Phys. **A219**, 157 (1974).
[24] R.E. Azuma et al., Phys. Rev. C **81**, 045805 (2010).
[25] Berger, M.J., Coursey, J.S., Zucker, M.A., and Chang, J. (2005), *ESTAR, PSTAR, and ASTAR: Computer Programs for Calculating Stopping-Power and Range Tables for Electrons, Protons, and Helium Ions* (version 1.2.3). [Online]
Available: http://physics.nist.gov/Star. National Institute of Standards and Technology, Gaithersburg, MD.
[26] D.R. Tilley et al., Nucl. Phys. **A708,** 3 (2002).
[27] H. Atsumi, et al., Jour. of Nucl. Mat. **133,** 268 (1985).
[28] H. Atsumi, et al., Jour. of Nucl. Mat. **141,** 258 (1986).
[29] Z. Hu et al., Journal of Physics: Conference Series **505,** 012014 (2014).